Synthesis and Characterization of Diamond-like Carbon Coatings Deposited by Plasma Source Ion Implantation and Conventional Ion Beam Assisted Deposition Processes

by

Captain Brian M. Stout, U.S. Army

A thesis submitted in partial fulfillment of
the requirements for the degree of

MASTER OF SCIENCE

(Nuclear Engineering and Engineering Physics)

at the

UNIVERSITY OF WISCONSIN-MADISON

1999

TABLE OF CONTENTS

ACKNOWLEDGMENTS

I would like to thank Dr. James Hirvonen and Dr. Costas Fountzoulas of the U.S. Army Research Laboratory, Aberdeen Proving Ground, Aberdeen, Md, for the use of their facilities and a good deal of their time. I greatly appreciate the continued technical support of Kumar Sridharan and Paul Fetherston of the Plasma Source Ion Implantation Group without whose assistance I would never have been able to complete this project. I would especially like to thank Professor John Conrad, PSII Group Director and my major advisor, for giving me the resources to accomplish this undertaking. Finally, I wish to express my deepest appreciation to Sara, my wife, and my three children; Brent, Sanora, and Riley for their patience over the last several years of graduate school.

LIST OF TABLES

LIST OF FIGURES

LIST OF FIGURES (continued)

LIST OF ACRONYMS

AFM: Atomic Force Microscopy

CVD: Chemical Vapor Deposition

DLC: Diamond-Like Carbon

IBAD: Ion Beam Assisted Deposition

LVDT: Linear Variable Differential Transformer

PSII: Plasma Source Ion Implantation

PVD: Physical Vapor Deposition

RBS: Rutherford Backscattering Spectrometry

Si-DLC: Silicon containing Diamond-Like Carbon

ABSTRACT

Diamond-like carbon coatings produced by Plasma Source Ion Implantation (PSII) and beamline Ion Beam Assisted Deposition (IBAD) were synthesized and studied. Gas pressure and electrical current were used as variables to design four independent PSII test sets. Beamline IBAD samples were produced with a pre-optimized set of parameters.

Profilometry measurements showed the films to have thicknesses between $1.44 \pm .09$ and $1.64 \pm .04$ μm and to possess very low roughness averages, ranging from 14 ± 3 to 28 ± 3 nm, which correlate with substrate surface roughness. Atomic Force Microscopy revealed that diamond-like carbon crystal sizes varied significantly with chamber pressure. Crystals were generally spherical in shape suggesting that films were highly amorphous. Microhardness and nanohardness test results showed the hardest films to be greater than 3 times the hardness of untreated steel. The elastic modulus of the films, measured during the nanohardness test, was directly related to film hardness. Fretting wear and Pin-on-Disk tests were performed to quantitatively assess the ability of films to resist wear. Fretting wear tests showed a dramatic decrease in friction for diamond-like carbon films with friction levels ranging from 10% to 30% of that of untreated steel. Pin-on-Disk tests revealed a significant improvement in wear resistence prior to stylus penetration into the substrate.

INTRODUCTION

Diamond-like carbon (DLC) films are defined as polycrystalline coatings consisting of a dense network of high density carbon (diamond) crystallites.[1] The term generally refers to a family of thin films related more by their inherent properties (i.e. hardness and wear resistance) than the method by which they are deposited on surfaces. For the purpose of this research, "DLC" encompasses all variations cited in much of the current literature as amorphous diamond-like carbon films (a-C:H), amorphous hydrogenated carbon-nitrogen film (a-C:H:N), amorphic diamond film (a-(C-C)), or any other of the many forms due to composition or production method.

Deposition techniques for DLC films are subdivided into two categories; physical vapor deposition (PVD) and chemical vapor deposition (CVD). PVD utilizes ion beam/plasma techniques to bombard target substrates with various forms of carbon ions during deposition. CVD processes apply polycrystaline films under high temperature and low pressure conditions. The processes associated with PVD and CVD have been described in numerous publications.[2,3,4]

Regardless of the deposition method, all DLC films have some combination of strong, covalent sp^2 (graphite) and sp^3 (diamond-like) hybridization bonding. In sp^2 bonding, three of the four valence electrons of the carbon atom form trigonal planar σ bonds at 120°. The remaining valence electron lies in the p_z orbital and forms a weaker π bond. In sp^3 hybridization bonding, each of the carbon atom's four valence electrons are located at the corner of a tetrahedron and form strong σ bonds at 109.5° with adjacent atoms. Generally,

the higher the sp^3/sp^2 ratio, the greater the degree of enhancement of mechanical and physical properties.

DLC films were first examined and documented in 1971 by Aisenberg and Chabot.[5] They deposited diamond-like carbon films onto a negatively biased (-40 to -100 V) substrate using an ion beam that resulted in amorphous, adherent, transparent, and relatively hard films. Over the succeeding two decades diamond-like carbon films have been researched and used for numerous industrial applications because of their high hardness, high degree of chemical inertness, and low friction.

More recently, numerous researchers have investigated the characteristics of diamond-like carbon films enhanced with silicon (Si-DLC) to further enhance hardness and to maintain low friction coefficients in humid environments.[6,7,8] For example, Hirvonen and Fountzoulas of the Metals Research Branch at the U.S. Army Research Laboratory applied an Ar+ beam at 40 keV using tetraphenyl-tetramethyl-trisiloxane $(C_6H_5)_4(CH_3)_4Si_3O_2$ molecules (Dow-Corning Type 704 Diffusion Pump Oil) as a precursor to deposit Si-DLC onto silicon and steel substrates.[9] Tribological testing showed the films to possess high hardness, low friction coefficients and improved wear resistance. Furthermore, the films could be produced with less demanding and more cost effective deposition methods.

The invention of Plasma Source Ion Implantation (PSII), a non-line-of-sight process, by Conrad *et al* in 1988 overcame the problems associated with deposition uniformity and target manipulation that existed in previous processes.[10] Utilizing plasmas to accelerate

different types of ions onto negatively biased substrates in PSII, DLC films could readily be produced at relatively low energies (2 to 10 keV) using methane or acetylene plasmas.[11]

The goal of this research is to quantitatively evaluate the DLC films produced by PSII to identify how the most significant parameters impact coating quality. The research also includes an assessment of Si-DLC produced by ion beam assisted deposition (IBAD) at the U.S. Army Research Laboratory at Aberdeen Proving Ground, Aberdeen, Md.

EXPERIMENTAL PROCEDURE

Substrate Selection and Preparation

Why 4140 Steel?

4140 steel was selected as the test substrate for DLC research primarily because of its broad range of industrial uses. Major applications for the steel are in the production of machine parts such as crank shafts, steering knuckles, axles, oil drilling bits, piston rods, pump parts, high pressure tubing, large industrial gears, flanges, wrenches, sprockets, and studs.[12] It is classified as a medium carbon, low-alloy steel. The composition of 4140 steel is shown in Table 1.

Table 1. Composition of 4140 Steel	
Element	**Percentage by Weight**
Iron (Fe)	~ 97.0
Chromium (Cr)	0.80 - 1.10
Manganese (Mn)	0.75 - 1.00
Carbon (C)	0.38 - 0.43
Silicon (Si)	0.20 - 0.35
Molybdenum (Mo)	0.15 - 0.25

Silicon content is added to avoid embrittlement at low temperatures during tempering. Chromium and molybdenum additions increase the hardenability by allowing for the formation of martensite at lower cooling rates from the austenitizing temperature. Upon subsequent tempering, these elements react with carbon to form a fine dispersion of

carbides that impart hardness to the steel. The presence of manganese is a result of the steel-making process.

Substrate Preparation

The 4140 steel substrate coupons used for this research were 1" in diameter and .25" thick with a hardness of 3.25 GPa. They were cut from an annealed bar procured from Wisconsin Metals, Reedsburg, Wi. The coupons were sanded smooth and polished to a mirror finish using a 1μm diamond paste during the final step. They were cleaned ultrasonically for 20 minutes in a bath of acetone to remove any residual oil and grease deposits. The polished and cleaned samples were then mounted on a steel plate with silver paint. The silver paint ensured good conductivity during PSII-DLC deposition. The steel plate was then itself mounted on the cathode platform inside the PSII chamber as shown in Figure 1.

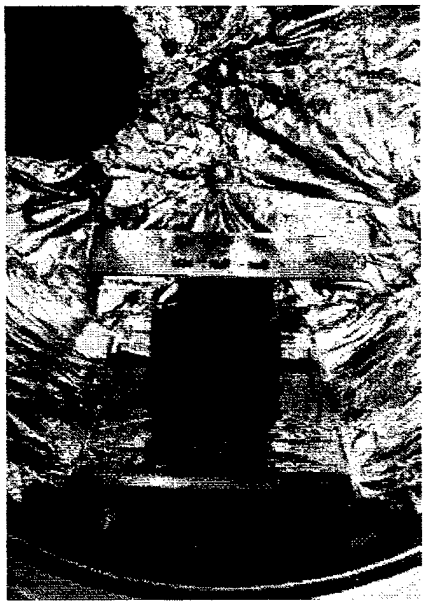

Figure 1. Steel Plate and Coupons Mounted on the Cathode in the PSII Chamber

The chamber was pumped down to a base pressure of $\sim 10^{-7}$ Torr and the coupons were sputter cleaned in Argon for one hour at 5 keV with a sputtering dose of from 2 - 5 x 10^{16} ions/cm^2 to remove any residual oxide layers.[13]

Preparation of 4140 steel coupons for the IBAD Si-DLC process was essentially the same as that of the PSII samples. The only procedure that varied from that which has already been mentioned was the sputter cleaning method. For the IBAD process, the samples were sputter cleaned with a directed Argon ion beam at 40 keV.

PSII-DLC Process Description

PSII utilizes several techniques including electron impact, glow discharge, and radio frequency for producing plasmas.[14] Glow discharge was the method used for the application of DLC coatings for this experiment.

During the glow discharge process, the target samples and chamber are prepared as described earlier. A carbon rich gas such as methane (CH_4) or acetylene (C_2H_2) is pumped into the chamber at a pressure on the order of 10^{-4} Torr. High voltage pulses at relatively low energies on the order of 5 to 10 keV are then applied to the cathode at a frequency ranging from < 1 to 300 Hz with a pulse length ranging from 25 to 150 μsec (Figure 2).

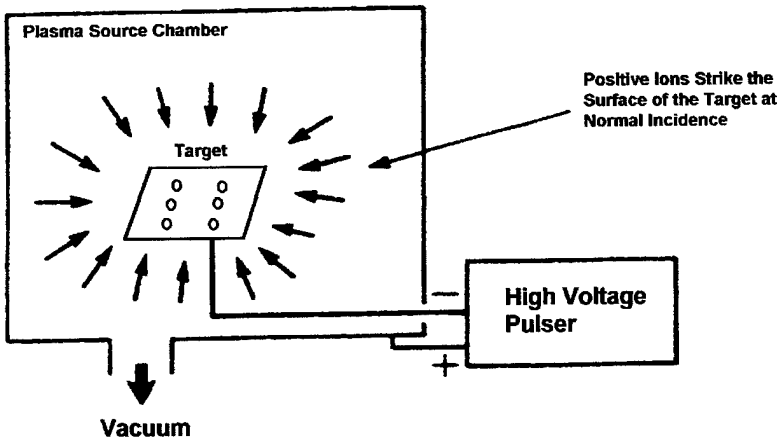

Figure 2. The PSII-DLC Process (Conrad)

At the initiation of each pulse, energetic electrons emitted from the cathode ionize the atoms of the neutral gas and a plasma sheath forms around the target platform. The ions in the plasma are accelerated through the sheath and strike the target platform creating a combination

of sp^2 (graphite-like) and sp^3 (diamond-like) bonds. The bonding process has been thoroughly described by Kerwin *et al.*[15] As ions strike the target further ionization takes place as secondary electrons are ejected and make their way to the outer chamber walls where most of the electrons are lost.

The voltage and current traces from an oscilloscope (Figure 3) isolate a single pulse of ionizing energy. The initial voltage spike at the far left is that portion of the pulse (approximately 5 μsec) which initiates the plasma. The total pulse width was 75 μsec. The current trace represents the net current from ions striking the target and electrons being absorbed at the wall. The bottom trace is a summation of the area under the current trace in units of μVsec.

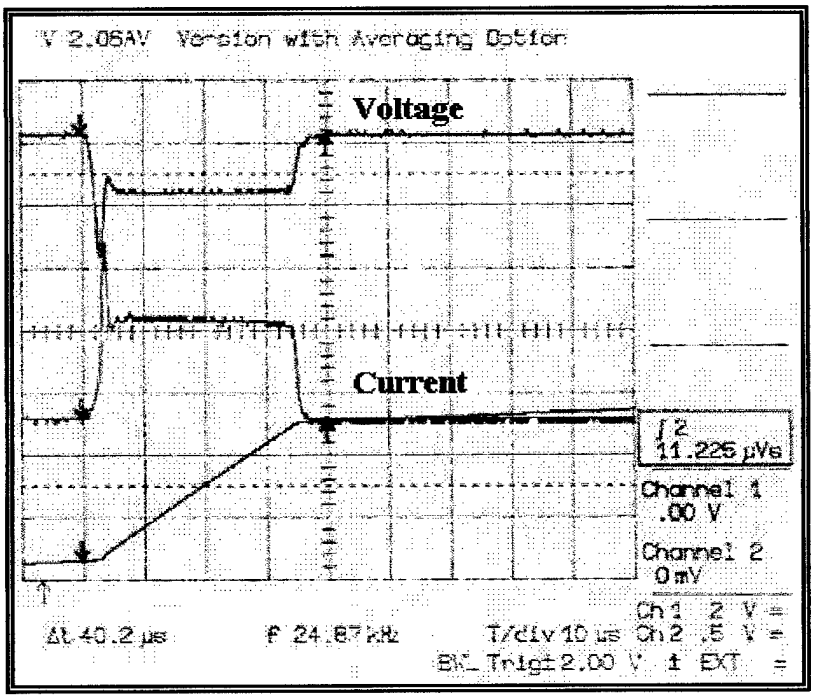

Figure 3. A Tyical Oscilloscope Trace of Voltage and Current Pulses for PSII-DLC.

IBAD Si-DLC Process Description

The IBAD process used to deposit Si-DLC for this research has been described in numerous publications.[16,17,18] The procedure, as it is performed at the U.S. Army Research Laboratory in the Materials Research Branch utilizes a 40 keV Ar+ beam from a Zymet 100 non-mass analyzed ion implanter.[19] Figure 4 shows the process in which the bombardment of the target by an ion beam combines with evaporative deposition.

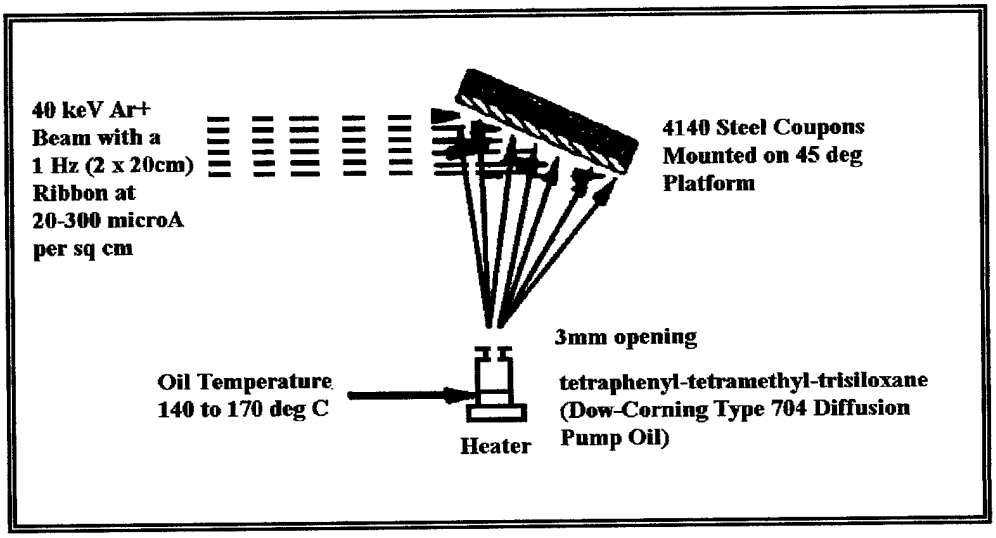

Figure 4. IBAD Si-DLC Deposition Process (Fountzoulas)

Tetraphenyl-tetramethyl-trisiloxane $[(C_6H_5)_4(CH_3)_4Si_3O_2]$, or Type 704 Dow-Corning diffusion pump oil, serves as the vapor precursor and is heated to temperatures ranging from 140° to 170° C.[20] The temperature controls the rate at which oil vapor is exposed to the ion beam and target. Heated oil vapor exits the heating element apparatus through a 3 mm nozzle at the top of the oil container. The substrate is positioned at a 45° angle with respect to the Ar+ beam and the vapor inflow. The oscillating (2 x 20cm) ion beam facilitates DLC growth with a current density between 20 and 300 $\mu A/cm^2$ corresponding to deposition rates varying from 0.1 to 0.3 $\mu m/hr$.[21]

Experimental Parameters

PSII-DLC Application

Many interdependent parameters impact the PSII process including, but not limited to applied voltage, pulse width, frequency, ion/electron current, neutral gas pressure, gas flow, substrate material selection, etc. This research focused on the effects of current and neutral gas pressure as shown in Table 2. Each set of parameters within the table is represented by a batch designator which will refer to parameters associated with that specific batch throughout the rest of this document. The table also displays parameters which were tracked but held as constant.

Table 2. PSII-DLC Parameters

Batch	Gas Pressure (mTorr)	Current (mAmps)	Voltage (kV)	Frequency (Hz)	Pulse Width (μsec)
PSII1	10	20	6.5	90	75
PSII2	10	10	6	90	40
PSII3	15	10	5	90	40
PSII4	15	20	5	90	75

High and low current values were selected along with high and low values for neutral gas pressure. These values were determined experimentally based on one-hour calibration runs which primarily established DLC uniformity and deposition rates for a given set of parameters.

Deposition rates were critical for calculating necessary run times to achieve a desired DLC coating thickness of 1.5 +/- .2 μm for each batch (Table 3). The importance of obtaining a uniform coating thickness was manifested in the need to draw valid

comparisons between different tribological and mechanical characterization tests.

Table 3. Deposition Rates and Calculated Run Times for Each Batch

Batch Designator	Deposition Rate (μm/hour)	Deposition Time (hours)
PSII1	.16	9.5
PSII2	.1	15
PSII3	.15	10
PSII4	.35	4.5

IBAD Si-DLC Application

The beamline IBAD Si-DLC process was performed by the U.S. Army Research Laboratory at Aberdeen Proving Ground, Maryland, under a single set of pre-optimized test conditions. Important parameters for the production of Si-DLC by the beamline IBAD process are shown in Table 4.

Table 4. IBAD Si-DLC Parameters

Deposition Parameter	
Supply Voltage	40 kV
Ion Beam Current	2.2 mA
Oil Evaporation Temperature	145° C
Deposition Time	2.5 hours

TESTS AND DISCUSSION

Film Characteristics

DLC Film Thickness

DLC film thickness was measured with the aid of Tencor Instrument's AlphaStep 200 and later verified at the Army Research Laboratory with a Tencor P-10 Surface Profiler (Version 1.6.5 software). Measurements were made on semi-masked silicon chips which were fastened to the mounting plate. The chips had been distributed in the general vicinity of the 4140 steel coupons prior to the deposition process (Figure 5).

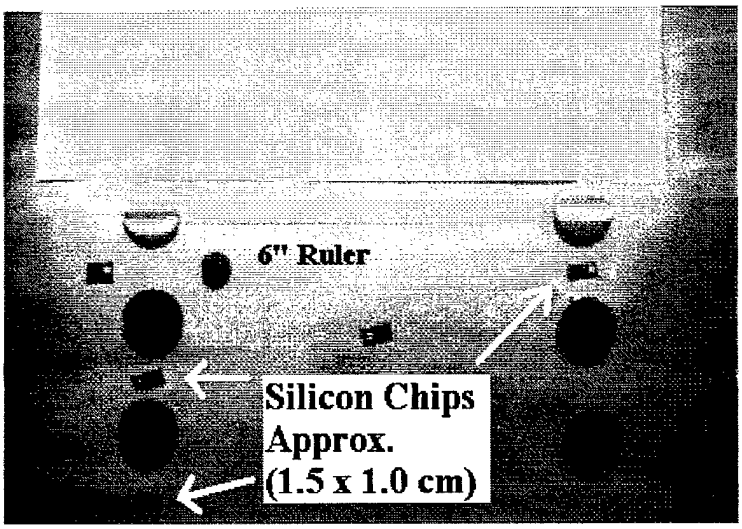

Figure 5. Si Wafers Distributed on the Deposition Platform

Five to seven different wafers from each batch were evaluated. After discarding the high and low measurements from each batch, the mean and standard deviation were calculated as shown in Table 5.

The beamline IBAD Si-DLC batch had a deposition time of 2.5 hours. Thickness measurements, made with the P-10 Surface Profiler, were taken directly from the coated 4140

steel coupons. Thicknesses ranged from 1.30 to 2.08 μm with the mean and standard deviation listed in Table 5 as well. Thicknesses deviate widely from the mean due to varying distances of individual substrates from the center of the oil vapor during the deposition process.

Table 5.	**Mean DLC Film Thicknesses**	
Batch	**Major Parameters**	**Mean Thickness (μm)**
PSII1	10 mTorr/20 mAmps	1.52 +/- .02
PSII2	10 mTorr/10 mAmps	1.52 +/- .07
PSII3	15 mTorr/10 mAmps	1.64 +/- .04
PSII4	15 mTorr/20 mAmps	1.54 +/- .15
Beamline IBAD Si-DLC	40 kv/145° C (oil temp.)	1.44 +/- .09

Average thicknesses coincided with the target thickness of 1.5 +/- 0.2 μm and were generally uniform across the target platform. The results suggest that DLC film deposition thicknesses can be controlled to a high degree of precision. The results also facilitate reasonable comparisons of other film characteristics based on similar thicknesses.

Roughness

Surface roughness plays an important role in tribological characteristics of coatings. It influences friction, surface microdeformation and consequently the wear mechanism of coatings. Furthermore, roughness is used to ensure components employed in numerous industrial applications meet design and operational requirements. For example, in orthopedic applications it has been noted that there is a direct correlation between wear debris generation and surface roughness. Another example is computer hard disks, where surface smoothness is extremely critical to successful performance.

A measurement of the roughness average was taken with a Tencor Instruments AlphaStep 200. The instrument utilized a unidirectional stylus to calculate average surface roughness (R_a) [ANSI Standard B46.1 - 1978, graphically determined] using the graphical centerline method as shown below.

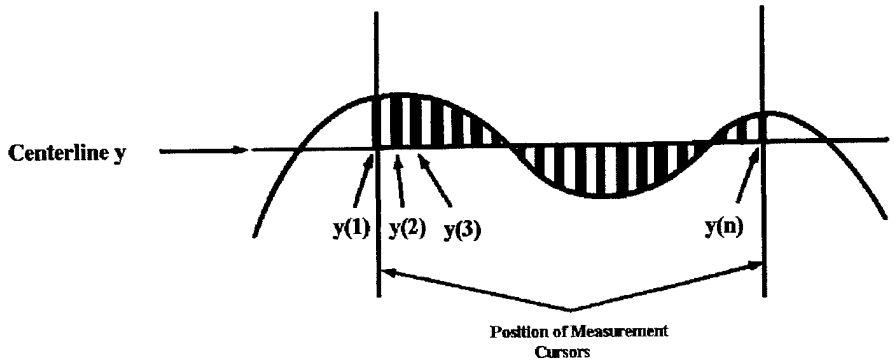

Figure 6. Graphical Determination of the Roughness Average by the AlphaStep 200[22]

By calculating the absolute value of between the position of the stylus at an incremental point

during the scan and the average value for y (marked as the centerline)distance, the roughness average was computed with the following formula:

$$R_a = \frac{y(1) + y(2) + y(3) + \ldots + y(n)}{n}$$

In this case the y(x) value is the deviation of each measured point from the centerline and n is the number of measurements taken between the cursors.

Roughness measurements were taken on DLC coated silicon chips and 4140 steel. Uncoated substrates were measured for comparison purposes. Scans were made over a distance of 2000 μm with a scanning increment of 1 scan per μm. Five measurements were taken for each sample and averaged. Tables 6 and 7 display R_a values for 4140 steel substrates and silicon substrates respectively.

Table 6. R_a Values for DLC on 4140 Steel	
Batch Number	**Mean Roughness Average (nm)**
Uncoated 4140 Steel	16 +/- 3
PSII1	28 +/- 3
PSII2	22 +/- 5
PSII3	17 +/- 6
PSII4	14 +/-3
Beamline IBAD Si-DLC	24 +/- 8

Table 7. R_a Values for DLC on Silicon	
Batch Number	**Mean Roughness Average (nm)**
Uncoated Silicon	11.1 +/- .58
PSII1	12.0 +/- .35
PSII2	12.4 +/- .48
PSII3	11.0 +/- 1.06
PSII4	12.0 +/- 1.07
Beamline IBAD Si-DLC	Not Measured

DLC films deposited by PSII and IBAD proved to be quite smooth when compared to roughness average standards for common industrial applications presented by Song and Vorburger.[23] The surface roughnesses of the thin DLC films seem to replicate the surface roughness of the substrate. This conclusion is based on a comparison of the R_a values of the coated specimens to that of the uncoated substrates. The conclusion is further supported by the fact that silicon and 4140 steel samples from each batch were coated side-by-side under the same conditions. The greater variation in mean roughness averages for the 4140 steel specimens is most likely due to variations in the preparation of the 4140 steel substrates, which was performed by hand.

Atomic Force Microscopy

Atomic Force Microscopy (AFM) is an emerging method used for imaging at the atomic level. AFM utilizes a stylus tip mounted on a flexible spring that is scanned over the surface of the specimen. The tip performs multiple sweeps to scan a designated surface area. The force between the stylus and the surface of the material are reflected in the mounting spring and used as a feedback signal to form an image of the surface topography.[24]

AFM was performed with the TopoMetrix Inc. Explorer AFM (SPMLab V3.06.06). With this particular model, a 3 mWatt/670 nm laser beam is reflected off the spring operated stylus arm as it moves across the surface of the sample similar to the method shown in Figure 7.

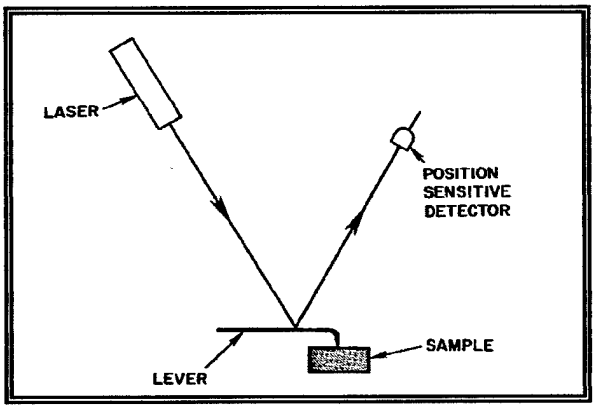

Figure 7. Functional Diagram of Optical Beam Deflection During AFM (Chen)

The deflected laser light is then collected by a segmented photodiode which detects the

position of the light as it changes. The scan range was set at 5.00 μm (scan area of 25.00 μm) with a scan rate of 35 μm/s and a resolution of 500 scans per micrograph. The resulting images are viewed from the top and are shown in Figures 8 through 13.

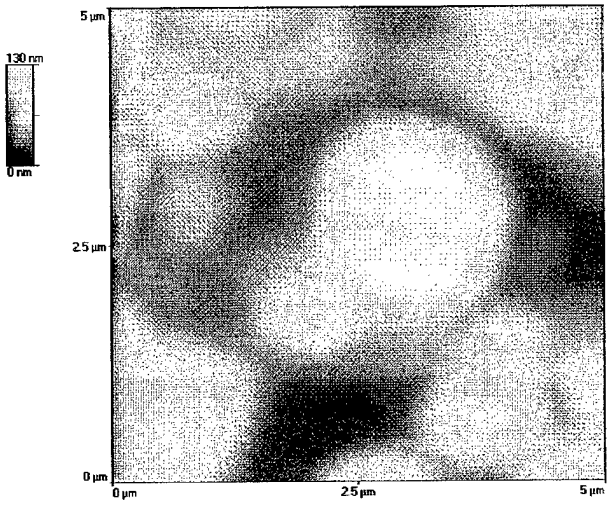

Figure 8. AFM Image of PSII-DLC (PSII1/ 10 mTorr/ 20 mAmps) on 4140 Steel

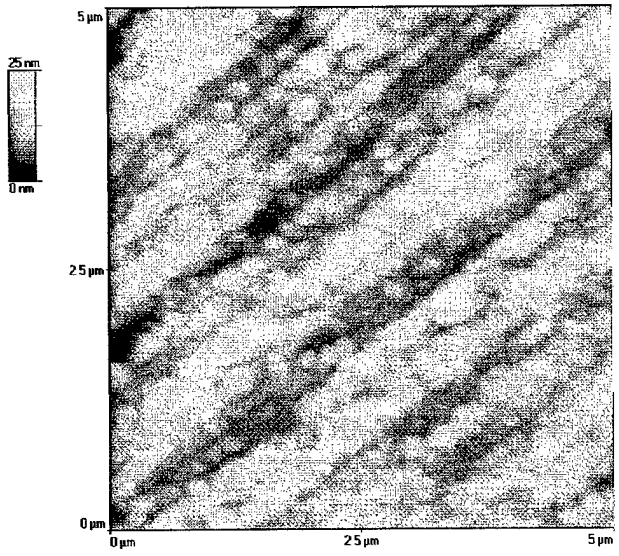

Figure 9. AFM Image of PSII-DLC (PSII2/ 10 mTorr/ 10 mAmps) on 4140 Steel

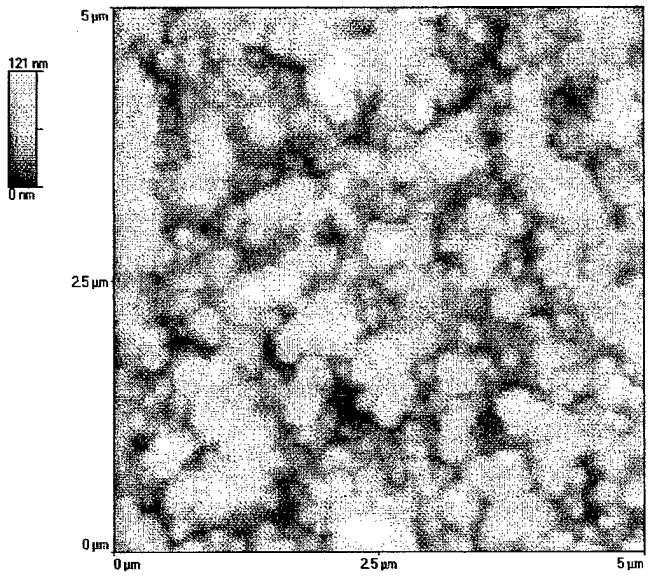

Figure 10. AFM Image of PSII-DLC (PSII3/ 15 mTorr/ 10 mAmps) on 4140 Steel

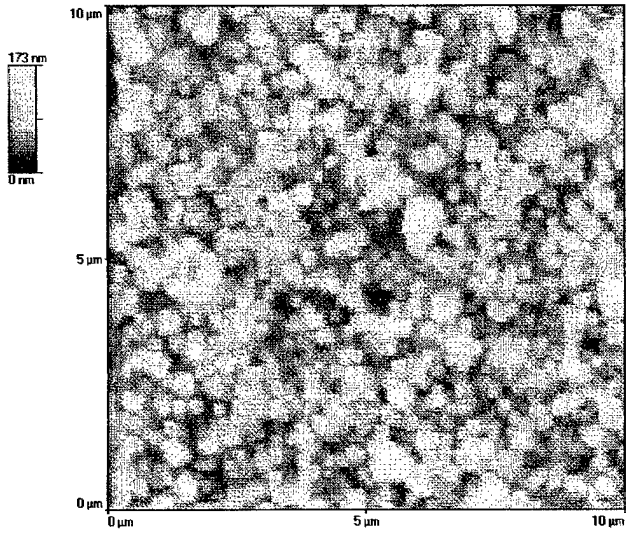

Figure 11. AFM Image of PSII-DLC (PSII4/ 15 mTorr/ 20 mAmps) on 4140 Steel

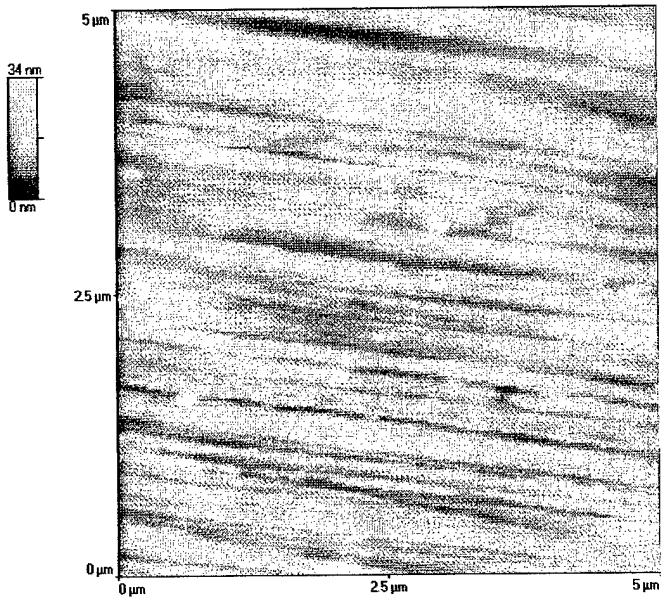

Figure 12. AFM Image of Uncoated 4140 Steel Substrate

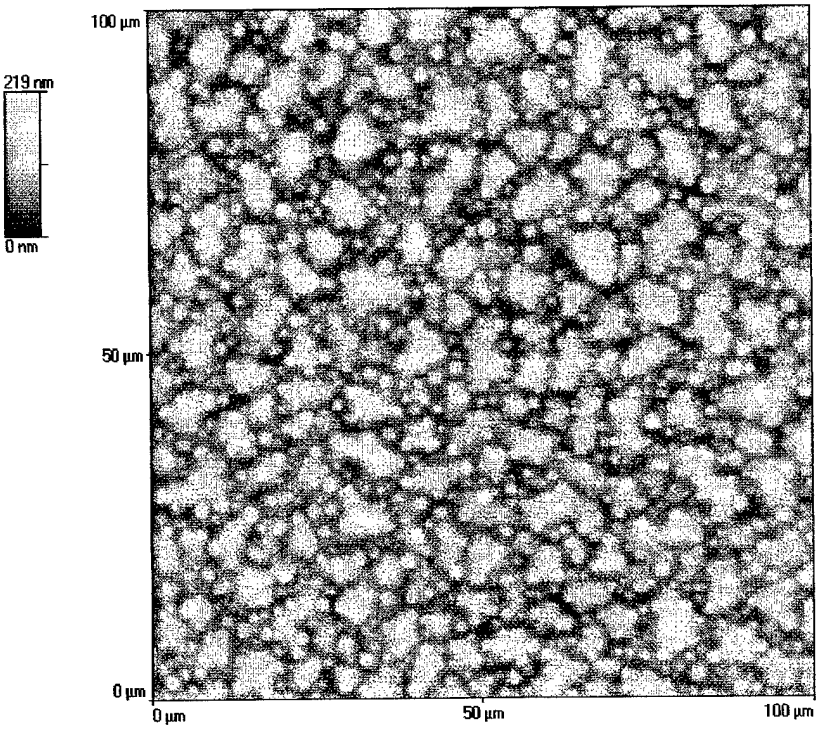

Figure 13. AFM Image of Beamline IBAD Si-DLC

Figure 12 represents the surface of an uncoated 4140 steel substrate in a polished condition. Spanning the entire horizontal length of the image are residual marks from a 0.5 μm diamond paste used in the final polishing step. Previous experiments have shown that similar grooves to promote adhesion of diamond films to the substrate.[25] Several raised spots at about 34 nm in height are either raised metal from the polishing process or foreign debris.

The generally spherical, raised projections in the remaining AFM images represent diamond crystal nucleation on the surface of the substrates. Previous studies have shown that AFM images exhibit a slight rounding at the edges of the crystalline images when compared to SEM micrographs.[26] This is primarily due to the fact that most AFM studies of diamond surfaces have been performed in air as opposed to a highly controlled vacuum environment. This condition has been known to create the potential for the absorption of water and other contaminants from the surrounding medium and has a slight affect on small scale imaging. Further analysis of AFM images has been performed under the assumption that general characteristics of the diamond crystals (i.e. size, shape, and density) are not significantly influenced by contaminants.

Diamond crystal sizes varied greatly by type of DLC. Observable diamond crystal sizes for the IBAD Si-DLC samples in Figure 13 ranged from ~ 1.1 μm to ~ 9.0 μm in diameter. They measured significantly larger than the PSII-DLC crystals which ranged in size from a maximum of ~ 2.0 μm in diameter for Figure 8 (PSII1/ 10 mTorr/ 20mA) to a minimum of ~ 0.1 μm in diameter for the other PSII-DLC batches. Crystal size was the

smallest in PSII4 (15 mTorr/ 20 mA) with an average diameter of ~ 0.3 μm. Previous research in this area using enhanced CVD and DC glow discharge techniques[27,28] suggest that as the molecular concentration of the hydrocarbon gas increases, DLC film grain size diminishes. With the exception of PSII1 (Figure 8) all PSII-DLC crystal sizes were comparable. Increased crystal size in PSII1 most likely can not be explained in terms of current, pressure, or deposition rate, but could possibly be due to some form of contaminant in the chamber such as residual moisture or gas.

PSII1 (Figure 8) and PSII4 (Figure 11) vary in pressure but have the same total current. As noted earlier, PSII1, with the lower pressure, has much larger and less dense crystal sites. The higher pressure in PSII4 promotes more nucleation sites and produces films with a smaller crystal size.

AFM images depicted the diamond crystals to be predominately spherical in shape. The only exception was found in PSII4 (Figure 11). In this case the diamond crystals were cubic. Kobashi *et al* [29] and Ravi[30] studied the morphology of diamond crystals produced by microwave enhanced plasma and combustion flame techniques respectively as a function of the amount of hydrocarbon to hydrogen and/or oxygen in the system. They independently confirmed that as the amount of hydrocarbon was increased compared to the amount of hydrogen and/or oxygen, the morphology of diamond crystals changed from a (111) orientation to a (100) orientation as shown in Figure 14. The depicted changes in the figure take place in a very narrow range of 0.4 % concentration for the transformation to occur. Although these results were attained with entirely different methods for producing DLC,

they suggest that there may have been a slight variation in the composition of the hydrocarbon gas or that there may have been a slight increase in contaminants such as moisture in the system. A small amount of oxygen is often found in PSII-DLC films during Rutherford Backscattering Spectrometry (RBS) testing as the result of either leaks in the vacuum or oxygen released from moisture in the chamber walls during the application process.

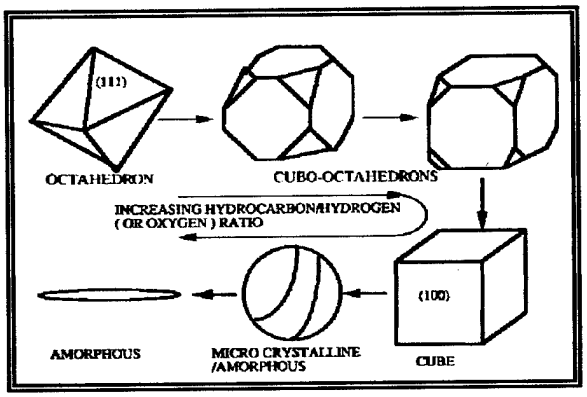

Figure 14. Morphology and Structural Transformations of Diamond as a Function of Hydrocarbon to Hydrogen and/or Oxygen Gas Mix (Ravi)

Previous studies of acetylene PSII-DLC films of comparable thickness (~900 +/- 50 Å) were performed by Muller at the University of Wisconsin in 1994.[31] RBS compositional analysis found the films to contain 52 +/-5 % C, 47 +/-5% H, and 1.0 +/-.1% O.

HARDNESS TESTING

Microhardness Indentation

Microhardness indentation testing is performed to assess mechanical properties of the surface by measuring the ability of a material to resist controlled penetration of an indenter into its surface. The process involves the application of a diamond indenter normally much harder than the material being tested. The coated specimen is mounted so that the indenter is pressed against the specimen perpendicular to its face with a specified normal force for a predetermined length of time. The indenter is then withdrawn and measurements of the residual indentation are used automatically by a digital microprocessor to calculate hardness values.

The Knoop microhardness indentation test was used for the testing of all coatings on 4140 steel coupons. This test, described thoroughly by Blau,[32] varies from other microhardness tests primarily due to the shape of the indenter (Figure 15) and the relative simplicity for calculating hardness. The indenter, because of its shape, produces comparably long and shallow indents which facilitate less cracking and shallow substrate penetration of thin films. It has an additional advantage in that the only measurement required to determine hardness is the length of the major diagonal, D, shown below.

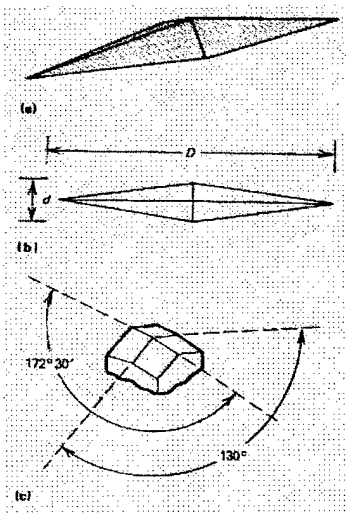

Figure 15. Knoop Indenter Tip [Blau] (a) 3-D view of tip (b) Diagonals D and d, where ratio D/d is 7.1143 (c) Major (172.5°) and minor (130°) apex angles.

Testing was performed using a Buehler MICROMET II Digital Microhardness Tester (UW Serial Number U552268). A load of 25 grams was applied for 15 seconds to each sample. This load was selected to prevent penetration by the indenter of more than half the distance through any DLC coating (~1.5 μm thick). Three specimens were selected from each batch and at least three hardness measurements were taken on each sample.

The digital microprocessor calculated the Knoop microhardness value. This calculation first involved the manual measurement of the major diagonal, D, as shown in Figure 15.[33] The Knoop hardness value, H_k, appearing on the digital readout can then be converted to GPa by applying the conversion factor of 0.00981 Gpa/H_k.

An alternate method for calculating the microhardness is presented by Blau. The following formula is based on the geometry of the indenter and the size of the indentation.

$$\mathbf{H = C_k (L/D^2)}$$

In this case, H is the hardness in Gpa, L is the load applied in grams, and D is the major diagonal length in μm. C_k is the Knoop constant with the value of 1.396×10^2 which takes into account the geometry of the indenter, the units of the applied load, and the conversion to units of GPa. A comparison of the two methods resulted in values that did not vary until the fourth decimal place in GPa.

Experimental results are listed in Table 8.

Table 8. Microhardness Test Results	
Batch Parameters	**Hardness [GPa]**
PSII1 (10 mTorr/ 20 mA)	10.099 +/- 1.463
PSII2 (10 mTorr/ 10 mA)	7.265 +/- 0.936
PSII3 (15 mTorr/ 10 mA)	7.031 +/- 1.678
PSII4 (15 mTorr/ 20 mA)	4.448 +/- 0.937
Beamline IBAD Si-DLC	6.348 +/- 1.245
Uncoated 4140 Steel	3.249 +/- 0.167

The value in the hardness column of Table 8 represents an experimental mean for 9 to 12 independent measurements of representative samples from each batch. Based on experimental means, PSII1 showed to have substantially higher hardness values. A graph of the percentage increase in hardness shows the relative improvement in hardness over that of uncoated 4140 steel.

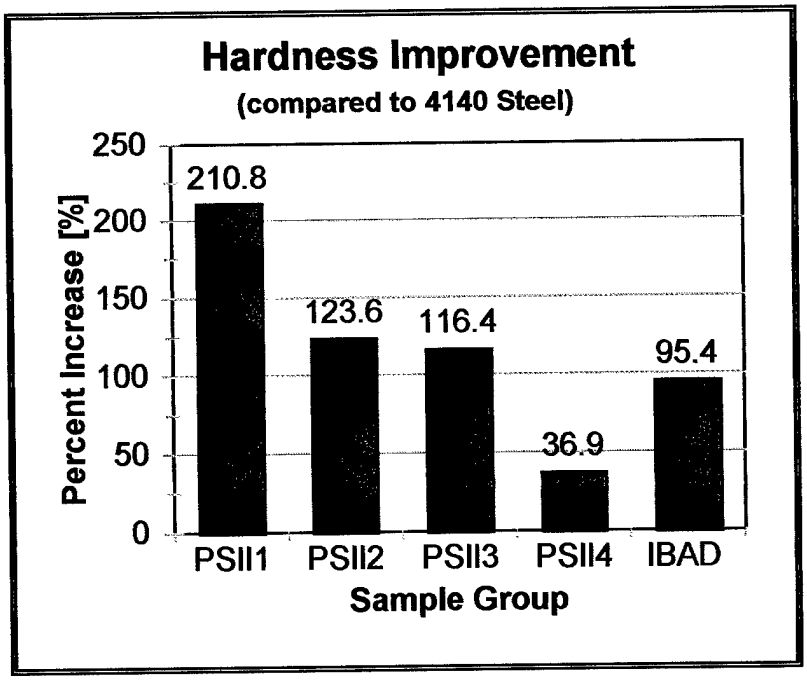

Figure 16. Relative Improvement in the Microhardness of 4140 Steel

The differences in hardness levels correlate with variances in deposition rates and the gas

pressure inside the chamber. Lower pressure corresponds to a decreased deposition rate. PSII1 and PSII2, with a chamber pressure of 10 mTorr, had deposition rates of .16 μm and .10 μm per hour respectively. PSII4, with a chamber pressure of 15 mTorr and an applied current of 20 mA, had a comparably high deposition rate of .35 μm per hour. The lower pressures also result in films of greater density and may be linked to the ratio of sp^2 to sp^3 bonds in the coating, although this has not been experimentally verified in this study.

Fountzoulas *et al*[34] link hardness in IBAD deposition of thin films to a low ion current (~20 $\mu A/cm^2$) and low oil temperatures (~150^0 C). These conclusions are based on tests performed on IBAD Si-DLCs deposited on M50 steel. Temperatures ranged from 150 to 170^0 C and the ion current density ranged from 20 to 250$\mu A/cm^2$ (Figure 17).

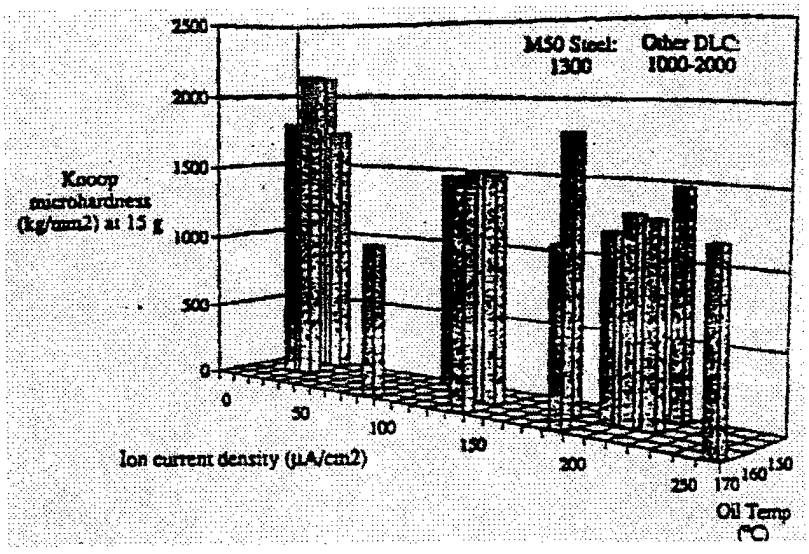

Figure 17. Knoop Hardness for Beamline IBAD Parameters (Fountzoulas)

Nanohardness Indentation

The process of nanohardness indentation testing creates and measures indents in materials which are too small to be evaluated with the optical microscope in the microhardness tester. It provides a more realistic value of hardness due to indenter depth control and increased sensitivity. In certain modes it also possesses the added capability of quantitative evaluation of the surface elasticity based on indenter penetration during the loading and unloading cycle.

Nanohardness indentation testing was performed to; (1) validate microhardness testing results, (2) compare measured hardnesses of identical DLCs deposited on silicon and 4140 steel, and (3) quantitatively assess the elasticity of the DLC coatings. Testing was performed at the Army Research Laboratory at Aberdeen Proving Ground, Md., with the Nano Indentor XP.

The basic operational concept behind nanohardness indentation involves an indentor applied in conjunction with a coil in a magnetic field, a depth sensor, and a loading controller. After specimens are mounted inside the chamber, the locations of the individual specimens are manually identified and programmed into the computer. Testing parameters specifying the target depth, the spacing and geometric configuration of the indents, and the time between individual measurements are then entered prior to execution of the test. The results for each indentation are in the form of a chart indicating the maximum depth, load, indent area, and the calculated values of the modulus and hardness (Figure 18). Additional data comes in the form of a plot of the load versus the indentation depth during the loading and unloading process.

File: MH064006.BIN Date: 1 Jul 1998 Page: 1
Specimen number: 006
Specimen name/Comments: Specimen 1-15 mT/20 mA

Hardness Experiment No. =1 Target Depth 800 nm
NOTE: ** bracketing indent number indicates data thrown out of Average.

Indent No.	Depth (nm)	Load (mN)	L/S^2 (nm^2/mN)	Area (nm^2)	Modulus (GPa)	Hardness (GPa)
22	8.54E+02	1.02E+02	5.80E+02	1.12E+07	1.11E+02	9.11E+00
23	8.46E+02	9.46E+01	6.37E+02	1.09E+07	1.03E+02	8.70E+00
24	8.46E+02	9.09E+01	6.28E+02	1.10E+07	1.01E+02	8.25E+00
21	8.41E+02	8.44E+01	6.45E+02	1.10E+07	9.55E+01	7.67E+00
Average	8.46E+02	9.30E+01	6.22E+02	1.10E+07	1.03E+02	8.43E+00
Std.Dev.	5.36E+00	7.29E+00	2.89E+01	1.28E+05	6.49E+00	6.17E-01

Figure 18. Computer Generated Nanoindentation Test Results

Testing was performed on silicon wafers coated in conjunction with the 4140 steel coupons. A minimum of five specimens were selected from each set of test parameters. Four indentations were made on each specimen separated by a distance of approximately 30 μm in a box configuration as seen in Figure 19.

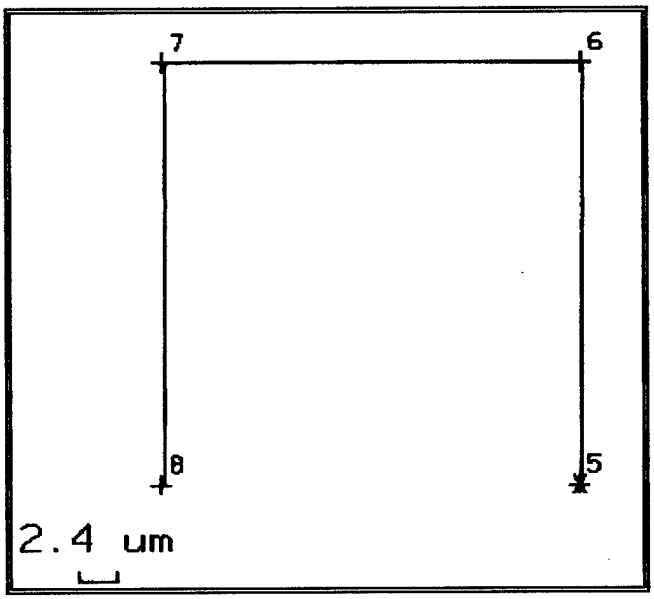

Figure 19. Geometric Configuration of Nanoindents

Nanohardness test results are shown in Table 9. The averages were determined by neglecting the high and low hardness and modulus value for each set of measurements.

Nanohardness Indentation Results		
Batch	**Hardness Ave (GPa)**	**Modulus (GPa)**
PSII1 (10mTorr/20mA)	10.78 +/- .30	130.6 +/- 2.62
PSII2 (10mTorr/10mA)	9.31 +/- 1.2	116.6 +/- 17.2
PSII3 (15mTorr/10mA)	7.44 +/- 1.15	104.3 +/- 10.5
PSII4 (15mTorr/20mA)	8.55 +/- .61	108.6 +/- 5.1
Beamline IBAD Si-DLC*	4.61 +/- .39	121 +/- 10.6

Table 9. Nanohardness Test Results for DLCs on Silicon Wafers (*Taken on 4140 Steel)

The calculations were based on measurements of the applied load of the indenter plotted against its indentation depth (with a target depth of 900nm) into the DLC coating. Nanohardness values are in agreement with the trends obtained from microhardness values shown in Table 8. The GPa values in Table 8 were computed from Knoop hardness values using a conversion factor. The lower hardness values in Table 8 compared to Table 9 are a result of substrate effects discussed earlier.

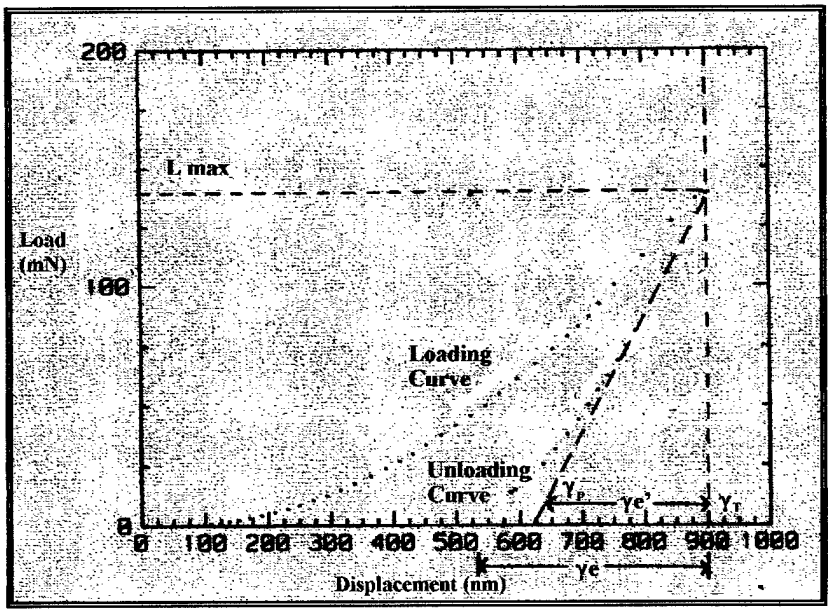

Figure 20. Load vs Indenter Depth During Loading and Unloading Cycle

Figure 20 represents measurements of the applied load versus depth for PSII1 (10mTorr/20mAmp). Also displayed in Figure 20 are graphical representations of quantities used to determine hardness and the modulus. The unloading curve differs from the loading curve due to partial elastic recovery taking place while the indenter is being retracted. Lmax is the maximum indenter load in mN. This is equal to the value of the y-intercept at the target depth of 900nm. γ_T represents the total indentation depth while γ_p and γ_e are the plastic and elastic portions of the total indentation depth respectively. Finally, γ_e' is the corrected value for the elastic portion of the indentation depth taken into account to adjust for the decrease in contact area as the indenter is being withdrawn.

Initially, the elastic recovery parameter (R), defined as γ_e/γ_p, is calculated with the following formula[35]

$$\mathbf{R = [(Lmax\ \gamma_T\ /2\ W_e) - 1]^{-1}.}$$

W_e represents the area of the elastic portion of the curve in Figure 20 corresponding to mechanical work released during the unloading cycle. For a homogeneous material, R is proportional to the ratio of the hardness (H) to the modulus. The "modulus" in this case is defined as[36]

$$\mathbf{modulus = E/(1-\nu^2).}$$

E is Young's Modulus and ν is Poisson's ratio. The hardness is then determined by the following formula[37]

$$\mathbf{H = \{2\ E\ R/[(1-\nu^2)(C\pi)^{-5}]\}.}$$

C is the geometric constant taking into account the size and shape of the individual indenter.

WEAR TESTS

Fretting Wear Test

The Fretting Wear test is designed to simulate damage to samples from small-amplitude oscillatory motion. The apparatus, as seen in Figure 21, is run by a controller unit connected to the testing equipment. The controller unit drives a stylus by electromagnetic means via a coil positioned in the field of a permanent magnet. The controller sends an electronic signal to the coil for establishing the frequency of oscillation. Amplitude readings measured through the LVDT (Linear Variable Differential Transformer) are then stored as data. The remainder of the apparatus, including the fulcrum, sliding weight and loading cam, ensure that the specimen stays stationary and in continuous contact with the stylus during testing.

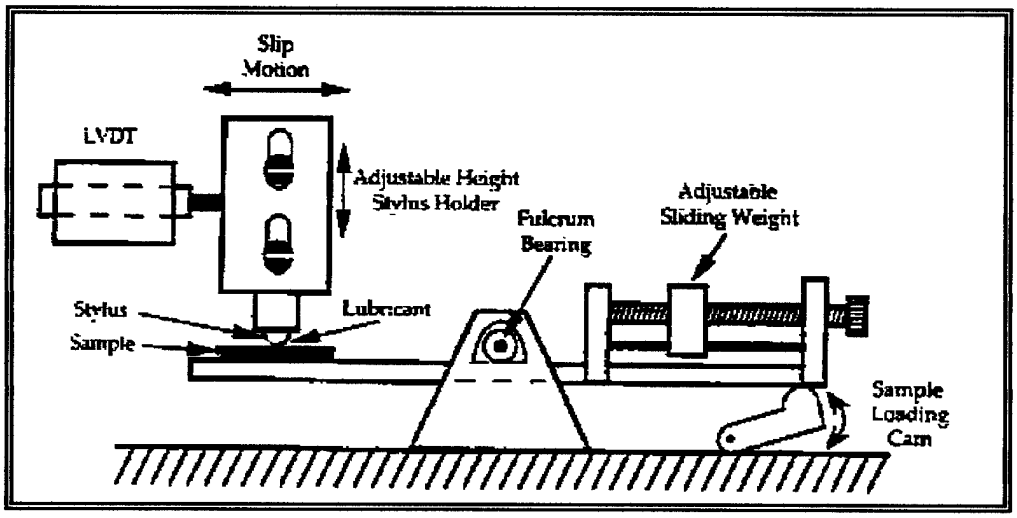

Figure 21. Fretting Wear Apparatus[38]

The Fretting Wear controller unit programming incorporated the parameters displayed in Table 10.

Table 10. Fretting Wear Parameters	
Parameter	
Stylus Material (Radius)	Ruby Ball (1.5mm)
Lubrication	No
Applied Load Force	50 grams
Average Contact Stress	903 MPa
Amplitude of Displacement	100 μm
Frequency of Oscillation	37.40 Hz
Number of Cycles	50,000

Three specimens were selected from each set of DLC parameters as well as from a single group of uncoated 4140 steel coupons. Samples were cleaned with acetone to remove any foreign surface material and mounted on the testing platform with double-sided tape to reduce the probability of slippage.

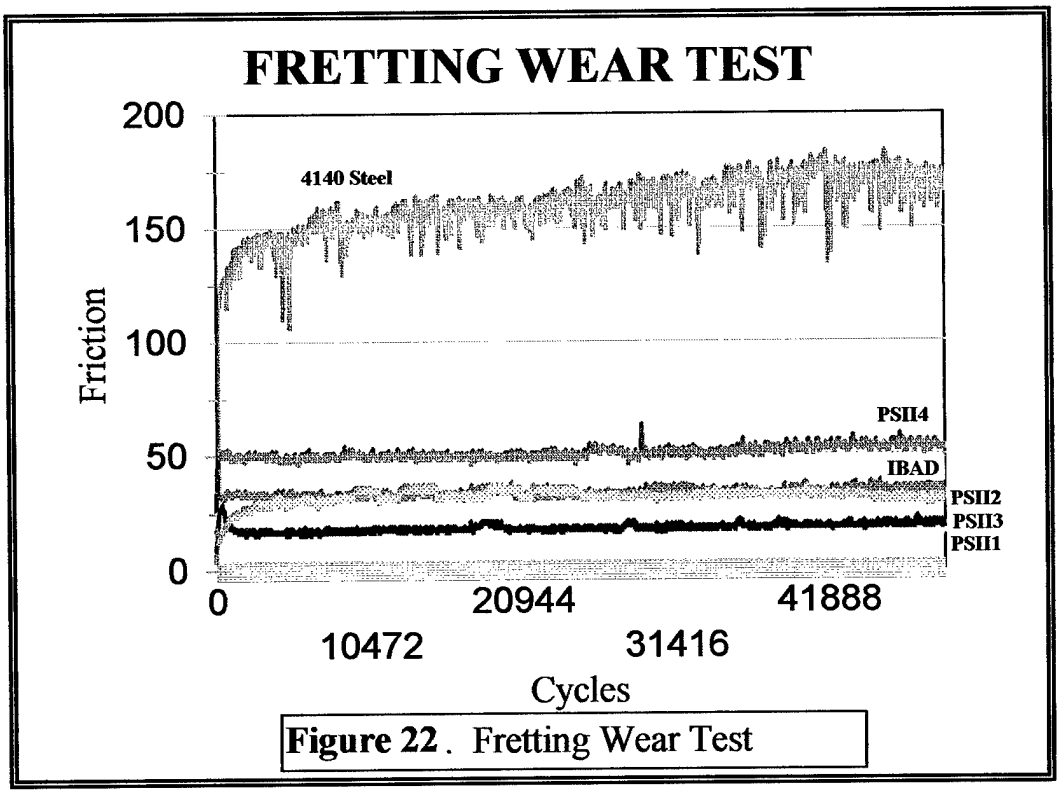

Figure 22. Fretting Wear Test

Test results were returned in the form of an arbitrary friction measurement corresponding to the progressive number of cycles associated with the measurement and plotted in Figure 22. Data was reported over a period of 1342 seconds. It was averaged from three separate tests for each group of DLC parameters. Ranges for arbitrary friction measurements by batch of samples are listed in Table 11.

Table 11. Fretting Wear	**Friction Ranges**	
	(Arbitrary Units)	
Group	**Low**	**High**
Uncoated 4140 Steel	114	180
PSII1 (10mTorr/20mA)	11	28
PSII2 (10mTorr/10mA)	16	26
PSII3 (15mTorr/10mA)	13	38
PSII4 (15mTorr/20mA)	47	53
Beamline IBAD Si-DLC	31	37

All DLC fretting wear results remained relatively constant after the initial contact (represented by the first 50 to 100 cycles of the graph). This points to the conclusion that breakthrough to the substrate material did not occur for any of the DLC specimens. Breakthrough would have been represented by sharp increases in the relative friction levels which would have eventually matched that of the uncoated 4140 steel. PSII1 and PSII3 displayed the lowest level of friction at approximately 10% and 12% of the friction level of uncoated 4140 steel respectively. The remaining DLC specimens also showed significant decreases in the friction level ranging from 18 to 30% of that of plain steel.

Pin-on-Disk Test

The pin-on-disk tribology test is used to simulate repetitive wear on a surface under controlled conditions. The testing apparatus, as seen below in Figure 23, consists of an indenter (a ruby ball of radius 1.5 mm) mounted on a gimbaled arm, a turntable, a variable speed controller, and an attached timer.

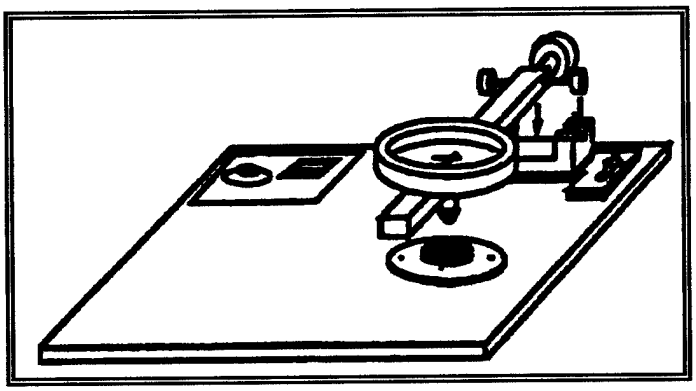

Figure 23. Pin-on-Disk Apparatus[39]

Testing was performed with the following parameters:

Table 12.	**Pin-on-Disk Parameters**
Parameter	
Load	100 grams
Lubrication	No
Contact Stress	1138 MPa
Speed	40 rpm (22.6 mm/sec)
Total Distance	13.571 m
Time	10 min
Temperature	68 deg F/20 deg C
Atmosphere	Laboratory Air

Testing was done on two specimens selected from each set of DLC parameters as well as a

pair of uncoated 4140 steel coupons.

Prior to the procedure, specimens were cleaned with acetone to remove any surface debris. They were mounted on the turntable with double-sided tape to prevent slippage during testing. The stylus was then loaded into the arm which together were balanced to ensure a perpendicular contact angle and uniform wear track.

The resulting wear scar for each specimen was measured using Tencor Instrument's AlphaStep 200 profilometer. Assuming that there was no significant pin wear, the volume lost during the procedure was then calculated using the following formula:[40]

$$\textbf{Volume Lost} = 2\,\pi\,R\,[r^2 \sin^{-1}(d/(2r)) - (d/4)(4r^2 - d^2)^{.5}]$$

where R = the wear track radius
d = wear track width
r = stylus end radius

Measurements of the wear track width ranged from 30 to 85 μm for the coated specimens and 130 to 210 μm for the uncoated 4140 steel coupons. The wear track radius was constant at 5.4 mm and the radius of the ruby stylus point was constant at 1.5 mm. The average for each specimen was then calculated by dropping the high and low measurement from each test run. The resulting averages are shown below in Table 13 and Figure 24.

Table 13.	Pin-on-Disk Results
Specimen Group	Avg. Volume Lost (mm^3)
PSII1	0.00737
PSII2	0.0094
PSII3	0.00491
PSII4	0.00352
Beamline IBAD Si-DLC	0.00374
Uncoated 4140 Steel	0.05473

Table 13. Pin-on-Disk Test Results (Average Volume Lost)

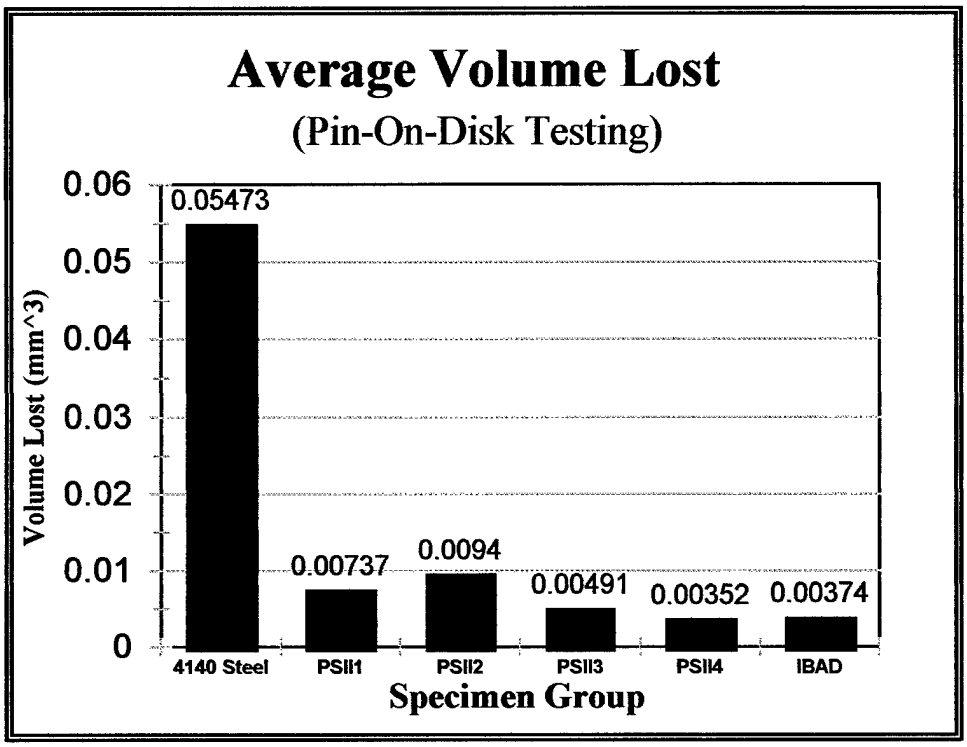

Figure 24. Average Volume Lost During Pin-on-Disk Testing by Specimen Group.

All DLC samples showed a significant improvement in wear resistence when compared to plain 4140 steel. PSII4 displayed a slightly lower volume of loss when compared to the other DLC coatings. The difference, however, was not significant.

SUMMARY

A summary of DLC film characteristics and test results are shown in Tables 14 and 15 respectively.

Table 14. DLC Film Characteristics

Batch	Major Parameters (mTorr/mAmps)	Dep. Rate (μm/hr)	Film Thickness (μm)	R_a (Steel) (nm)	R_a (Silicon) (nm)
Plain 4140 Steel	N/A	N/A	N/A	16 ± 3	11.1 ± .58
PSII1	(10 mTorr/20 mAmps)	.16	1.52 ± .02	28 ± 3	12.0 ± .35
PSII2	(10 mTorr/10 mAmps)	.1	1.52 ± .07	22 ± 5	12.4 ± .48
PSII3	(15 mTorr/10 mAmps)	.15	1.64 ± .04	17 ± 6	11.0 ± 1.06
PSII4	(15 mTorr/20 mAmps)	.35	1.54 ± .15	14 ± 3	12.0 ± 1.07
IBAD Si-DLC	40 keV/ 145° C	.58	1.44 ± .09	24 ± 8	N/A

Table 15. Summary of Test Results*

Batch	Microhardness (GPa)	Nanohardness (GPa)	Modulus (GPa)	Rel Friction Av. (Arb Units)	Wear Resistance (Vol Loss[mm^3])
4140 Steel	(6) 3.249±.167	N/A	N/A	(6) 159	(6) .05473
PSII1	(1) 10.099± 1.463	(1) 10.78±.30	(1) 130.6±2.62	(1) 15	(4) .00737
PSII2	(2) 7.265±.936	(2) 9.31±1.2	(3) 116.6±17.2	(2) 18	(5) .0094
PSII3	(3) 7.031±1.678	(4) 7.44±1.15	(5) 104.3±10.5	(3) 32	(3) .00491
PSII4	(5) 4.448±.937	(3) 8.55±.61	(4) 108.6±5.1	(5) 51	(1) .00352
IBAD	(4) 6.348±1.245	(5) 4.61±.38	(2) 121±10.6	(4) 34	(2) .00377

* The "(number)" represents the associated ranking in each category.

CONCLUSION

1. All DLC coatings showed a marked improvement in hardness, relative friction, and wear resistance.

2. The harder PSII-DLC films were those produced at the lower pressure of 10 mTorr. A significant increase in hardness was seen in PSII1 at 10 mTorr and 20 mAmps. The DLC with the least improvement was PSII4 at 15 mTorr and 20 mAmps. This low hardness level is most likely related to its relatively fast deposition rate which leads to lower density films.

3. There is an excellent correlation between microhardness and nanohardness test results. As expected, however, there is evidence of greater substrate effects in the microhardness test.

4. The elastic modulus was determined for all DLC coatings using the nanohardness test. This value, with the exception of the IBAD Si-DLC, was directly related to the corresponding hardness value.

5. Fretting wear results show a dramatic decrease in friction for DLC films.

6. Pin-on-Disk testing shows that there is a substantially higher wear resistance in DLC films prior to stylus penetration into the substrate.

7. Surface roughness values of DLC films were very low and exhibit a correlation with the substrate surface roughness. There is a possible correlation between high roughness average values and increased hardness.

8. Coating grain morphology is generally spherical. A comparison of AFM micrographs with previous studies indicates that such a morphology is characteristic of microcrystalline or amorphous structure.

9. Films produced by IBAD containing silicon were comparable to that of PSII-DLC.

Although other research has shown an enhancement in hardness and friction coefficients in films enhanced with silicon ions, this conclusion could not be ascertained from this specific research and analysis.

10. Si-DLC films produced by IBAD were more coarse in structure than PSII-DLC films. This is attributed to higher deposition temperatures and lower current density used in the processing of IBAD films.

11. This research has further solidified the already existing collaboration between the University of Wisconsin and the U.S. Army Research Laboratory and opened the door for more collaborative work in this area.

FUTURE WORK

This research should spark interest for future investigations in the following areas:

1. A qualitative study of PSII-DLC coatings produced with acetylene or methane ions to that of PSII-DLC enhanced with silicon ions.

2. Research in the area of DLC crystal structures; how crystal size, shape, and density of the films impact hardness, friction, wear and adhesion.

3. A comparative cost analysis of PSII-DLC and that produced by various CVD and PVD methods.

4. Studies of how DLC films and ion implantation in general could support Department of Defense activities ie. an analysis of potential applications and how reduced logistical requirements result from enhanced equipment lifetimes associated with DLC films.

5. The sp3/sp2 ratio for various PSII-DLC process parameters

6. How varying degrees of oxygen implanted during the PSII process impacts DLC film quality.

REFERENCES

1 P. Gielisse, Mechanical Properties of Diamond, Diamond Films, Diamond-like Carbon and Like-Diamond Materials, **Handbook of Industrial Diamonds and Diamond Films**, Ed. Mark A. Perlas, Marcel Dekker, New York, (1998)49-55.

2 M. Kitabatake and K. Wassa, *J. Appl. Phys.* 58(1985)1693-1695.

3 J.C. Angus, H.A. Will and W.S. Stanko, *J. Apply. Phys.* 39(1968)2915-2922.

4 K. Miyoshi, R.L. Wu, A. Garscadden and H. Jackson, *Int. Conf. on Met. Coatings and Thin Films Conf. Proc.*, San Diego, (1993)1-16.

5 S. Aisenberg and R. Chabot, *J. Appl. Phys.* 42(1971)2953.

6 K. Oguri and T. Arai, *J. Mater. Res.* 7(1992)6.

7 Fountzoulas, *et al.*, *Mat. Res. Soc. Symp. Proc.* 273(1993)845-850.

8 J. Fatkin, A. Kohno and N. Kanekama, *Jap. J. Appl. Phys*, 26(1987)856-862.

9 J.K. Hirvonen and J.D. Demaree, DoD Activities in Ion Beam Processing, **Advances in Coatings Technologies for Surface Engineering**, (1997)53-67.

10 J.R. Conrad, United States Patent No. 4,764,394 (1988).

11 Sridharan, *et al.*, *ASM-TMS Mat. Conf. Proc. Surface Modification Technologies IX*, Cleveland, (1995)401.

12 T.V. Philip and T.J. McCaffrey, Ultrahigh-Strength Steels, **Metals Handbook Vol.1, Properties and Selection: Irons, Steels and High Performance Alloys**, 10th ed., ASM International, (1990)432.

13 S. Malik, K. Sridharan, R.P. Fetherston, A. Chen and J.R. Conrad, *J. Vac. Sci. Technol.*, B 12(2)(1994)843-849.

14 J. Chen, J.R. Conrad and R.A. Dodd, *J. of Mat. Eng. and Perf.*, 2(1993)839-842.

15 D.B. Kerwin, I.L. Spain, and R.S. Robinson, *Thin Solid Films*, 148(1987).

16 J.K. Hirvonen, *Mat. Sci. Rep.*, North-Holland, 6(1991)215-274.

17 C.G. Fountzoulas, *et al.*, *Mat. Res. Soc. Symp. Proc.*, 273(1993)645-650.

18 M. Kitabatake and K. Wasa, Diamond and Diamond-like Thin Films Produced by Ion Beam Techniques, **Handbook of Ion Beam Processing Technology**, Ed. J. Cuomo, New Jersey, (1989)415-434.

19 C.G. Fountzoulas, T.Z. Kattamis, J.D. Demaree, W.E. Kosik, W. Franzen and J.K. Hirvonen, *J. Vac. Sci.Technol.*, B12(2) (1994)977-980.

20 C.G. Fountzoulas, *et al.*, *Mat. Res. Soc. Symp. Proc.*, 273(1993)645-650.

21 C.G. Fountzoulas, T.Z. Kattamis, and M. Chen, *Mat. Res. Soc. Symp. Proc.*, 316(1994)851-856.

22 Tencor Instruments, AlphaStep 200, Operation Manual, 35.

23 J.F. Song and T.V. Vorburger, Surface Texture, **ASM Handbook, Vol. 18, Friction Lubrication and Wear Technology**, ASM International, (1992)334-344.

24 C.J. Chen. **Introduction to Scanning Tunneling Microscopy**, New York, (1993)313-324.

25 K. Shibuki, M. Yagi, K. Saigo, and S. Takatsu, *Surface Coat. Tech.*, 36 (1988)295.

26 K. Rutledge and K. Gleason, Characterization Methods, **Handbook of Industrial Diamonds and Diamond Films**, ed. M. Perlas, New York, (1998) 451.

27 L.S. Plano, S. Yokota, and K.V. Ravi, *Proc. 1st Int. Symp. Diamond and Diamond-like Films* (The Electrochemical Society, Inc., Pennington, NJ, 1989) 380.

28 A. Ono, H. Baba, H. Funamoto, and A. Nishikawa, *Jpn. J. Appl. Phys.* 25, L803, (1986).

29 K. Kobashi, K. Nishimura, Y. Kawate, T. Horiuchi, *Phys. Rev.* B 38, 4067 (1988).

30 K. Ravi, C. Koch, H. Hu, A. Joshi, *J. Mat. Res.* 5 (1990) 2356.

31 D.E. Muller, A Study of the Composition, Structure and Properties of Amorphous Hydrogenated Diamond-like Carbon Films, Madison, (1994)32.

32 P.J. Blau. Microindentation Hardness Testing, **ASM Handbook, Vol. 18, Friction Lubrication and Wear Technology**, ASM International, (1992)414-418.

33 P.J. Blau. Microindentation Hardness Testing, **ASM Handbook, Vol. 18, Friction Lubrication and Wear Technology**, ASM International, (1992)416.

34 C.G. Fountzoulas, *et al.*, *Mat. Res. Soc. Symp. Proc.*, 273(1993)648.

35 H.M. Pollock. Nanoindentation, **ASM Handbook, Vol. 18, Friction Lubrication and Wear Technology**, ASM International, (1992)422.

36 Ibid., 422.

37 Ibid., 423.

38 P. Sandstrom. Fretting Wear Tester (Theory, Operation, and Maintenance), Engineering Research Center for Plasma Aided Manufacturing.

39 J.R. Conrad, *PSII Newsletter*, 1(1989)5.

40 Unk, Standard Test Method for Wear Testing with a Pin-on-Disk Apparatus, ASTM Designation: G99-90, ASTM Committee, (1990)399-403.